

1
2
3
4
5
6
7
8
9
10
11
12
13
14
15
16
17
18
19
20
21
22
23
24
25
26
27
28

Sediment deposition from turbidity currents in simulated aquatic vegetation canopies

M. Soler¹, J. Colomer¹, T. Serra¹, X. Casamitjana¹ and A. Folkard²

¹ Department of Physics, University of Girona, 17071, Girona, Spain

² Lancaster Environment Centre, Lancaster University, Lancaster LA1 4YQ, United Kingdom

Corresponding author: marianna.soler@udg.edu

ABSTRACT

A laboratory flume experiment was carried out in which the hydrodynamic and sedimentary behaviour of a turbidity current was measured as it passed through an array of rigid obstacles. The obstacles were intended primarily to simulate aquatic vegetation canopies, but could equally be taken to represent other things, for example forests or offshore wind turbines. The turbidity currents were generated by mixing naturally-sourced, poly-dispersed sediment into a reservoir of water at concentrations from 1 to 10 gL⁻¹, which was then released in the experimental section of the flume by removing a lock gate. For each initial sediment concentration, runs with obstacle arrays with solid plant fractions of 1% and 2.5%, and control cases with no obstacles, were carried out. The progress of the current along the flume was characterized by the array drag term, $C_D a x_{toe}$ (where C_D is the array drag coefficient, a the frontal area of cylinders per unit volume and x_{toe} the current toe position along the flume). The depositional flux of sediment from the current as it proceeded was measured at thirteen traps positioned along the flume. Analysis of these deposits divided

1 them into fine (2.2–6.2 μm) and coarse (6.2–104 μm) fractions. At the beginning of the
2 development, the gravity current proceeded in an inertia dominated regime until $C_D a x_{toe} = 5$.
3 And for $C_D a x_{toe} > 5$, the current transitioned into a drag-dominated regime. For both fine and
4 coarse sediment fractions, the rate of sediment deposition tended to decrease gradually with
5 distance from the source in the inertial regime, remained approximately constant at the early
6 drag-dominated regime, and then rose and peaked at the end of the drag-dominated stage.
7 This implies that, when passing through arrays of obstacles, the turbidity currents were able
8 to retain sufficient sediment in suspension to maintain their flow until they became
9 significantly influenced by the drag exerted by the obstacles.

10 **Keywords** gravity current, inertial regime, drag-dominated regime, sediment deposition,
11 canopy

1 INTRODUCTION

2

3 The dynamics of gravity currents have been studied for many years using lock exchange
4 experiments, in which two fluids of different densities within an experimental flume are
5 initially at rest and separated by a lock gate. When the gate is removed, differences in the
6 hydrostatic pressure cause the denser fluid to form a gravity current in one direction along
7 the bottom boundary of the tank, while the lighter fluid flows in the opposite direction above
8 it. Analysis of this flow configuration has been carried out theoretically, notably by Benjamin
9 (1968), and experimentally, notably by Simpson (1982) and Shin et al. (2004). The interface
10 between the two counter-flowing currents will be largely horizontal, but will curve sharply to
11 become near-vertical at their leading edges (Benjamin, 1968). In lock-release gravity
12 currents, three phases can develop, as observed by several investigations (e.g. Marino et
13 al., 2005; Adduce et al., 2012). In the first, inertial phase, the front's position varies as t^1 (i.e.
14 the front velocity is constant); this phase lasts until the motion is affected by reflections from
15 the back wall of the channel. In the second, self-similar phase, the relationship of the front's
16 position to time is dependent on the Reynolds number. In infinite lock release cases where
17 the Reynolds number is low enough that a linear drag law (i.e. the drag coefficient $C_D \sim 1/Re$)
18 can be assumed, it varies as $t^{1/2}$, whereas in cases where the Reynolds number is high
19 enough that the drag coefficient can be assumed constant, it varies as $t^{2/3}$. Ozan et al. (2015)
20 pointed out that currents which begin this phase in the high Reynolds number regime may
21 be slowed sufficiently by drag forces that they transition from the high Reynolds number
22 case to the low Reynolds number case during their evolution. The same authors also found
23 that, in LES models of gravity currents passing through arrays of horizontally-aligned
24 obstacles, the currents were not entirely self-similar (i.e. the positions of the front and body
25 of the current did not have the same dependence on time) because of mixing at the current's
26 interface with the ambient fluid. In their models, the front's position varied as $t^{3/4}$ rather than
27 the $t^{2/3}$ observed by others and predicted by shallow water theory. Finally, the currents may

1 transition to a third phase in which the dominant force balance is between viscous and
2 buoyancy forces, and the front's position varies as $t^{1/5}$.

3

4 The effects on lock-released gravity currents of bed roughness have also been studied by
5 recent laboratory and numerical investigations (e.g. La Rocca et al., 2008; Gonzalez-Juez et
6 al., 2009, 2010; Nogueira et al., 2013, 2014; and Bhaganagar 2014). The bed roughness
7 was found to affect the front propagation, the amount of entrainment of the ambient fluid into
8 the current and the current's ability to entrain sediments from the bed.

9

10 In many situations, there are substantive obstacles to gravity currents, and in these
11 situations the drag forces that these obstacles impose can dominate both inertial forces and
12 the drag due to the boundaries of the flow domain. Gravity currents may become drag-
13 dominated where they propagate into partially or fully vegetated channels, which have been
14 simulated in laboratory experiments by arrays of rigid cylindrical obstacles (Hatcher et al.,
15 2000; Tanino et al., 2005; Zhang & Nepf, 2008; Zhang & Nepf, 2011). Hatcher et al. (2000)
16 showed that gravity currents produced by finite volume release of a relatively dense fluid into
17 a relatively less dense ambient that flow through such arrays of obstacles decrease their
18 velocity as they proceed such that the position of the current front, x_c , evolves following:

$$19 \quad x_c \sim \left(\frac{q_0 \cdot g' \cdot d}{C_D \cdot \phi} \right)^{1/4} \cdot t^{1/2} \quad (1)$$

20

21 where q_0 is the total current volume per unit cross-flume distance; g' is the reduced gravity
22 $g' = g(\rho_c - \rho_a)/\rho_a$ (ρ_c and ρ_a are the current and ambient fluid densities respectively); d is the
23 individual obstacle width (cylinder diameter); $\phi = (\pi/4) \cdot a \cdot d$ is the volume fraction of the
24 obstacles; $a = Nd/A$ is the frontal area of cylinders per unit volume (Nepf, 1999), N is the
25 number of cylinders, A is the bed area occupied by the cylinder array; and finally C_D is the
26 array drag coefficient. C_D is a function of the cylinder Reynolds number $Re_c = |u|d/\nu$ (where ν
27 is the kinematic viscosity of the fluid, and u the toe velocity).. For smooth, isolated circular

1 cylinders and Re values in the range $1 - 10^5$, C_D is described by the empirical expression
 2 (White, 1991):

3

$$4 \quad C_D \approx 1 + 10.0 \text{Re}_c^{-2/3} \quad (2)$$

5

6 This expression holds for vegetation canopies in which the dimensionless array density, $ad <$
 7 0.03 (Nepf, 1999).

8

9 If situations where drag can be neglected, the gravity current evolution reduces to the classic
 10 un-obstructed release from an infinite lock, where the position of the current's front x is linear
 11 with time and the current propagates at a steady velocity that may be reasonably
 12 approximated as (Tanino et al., 2005),

$$13 \quad x_c \sim \left(\frac{g' \cdot H}{4} \right)^{1/2} \cdot t \quad (3)$$

14 After analysing an infinite lock release through obstacles, Tanino et al. (2005) obtained that
 15 drag forces dominate inertia, when the array drag is $C_D aL > 7$ (being L the current toe
 16 position along the flume, x_{toe} in the present study). In such case, the dependence of x is a
 17 power dependence with time, in accordance with Hatcher et al. (2000). This leads to a change
 18 in the shape of the interface between the gravity current and the ambient fluid. This interface
 19 is nearly horizontal during the inertial regime, but takes on a triangular side view profile in the
 20 drag-dominated regime (Tanino et al. 2005), such that the interface profile can be used as a
 21 criterion to classify flow regimes.

22

23 Turbidity currents are a subset of gravity currents, in which the density differences are due to
 24 differences between the concentrations of suspended particles in the two fluids. They occur
 25 commonly in nature, and may persist for long travel times and produce significant
 26 modifications of substrate characteristics via sediment scouring and deposition (Kneller and
 27 Buckee, 2000; Hogg and Woods, 2001; Felix, 2002). Unlike gravity currents where the

1 density differences are due to conservative properties of the fluid, such as salt concentration
2 or temperature, turbidity currents are complicated by the fact that they may entrain sediment
3 particles (by bed scouring) or lose sediment particles (by deposition), increasing or
4 decreasing, respectively, density differences that drive them as they propagate. The
5 propagation and deposition patterns of turbidity currents are governed by both their flow
6 structure and sediment characteristics (concentration and grain size). Aquatic examples of
7 these phenomena are found in reservoirs (Chikita, 1989), lakes (Roget and Colomer 1996;
8 Serra et al, 2002a; Serra et al., 2005; Soler et al., 2009), and oceans (Kneller and Buckee
9 2002; Felix, 2002; Meiburg and Kneller, 2010). In those turbidity currents it is necessary to
10 introduce a transport equation for the particle concentration to take into account that the
11 driving buoyancy force changes with time and position along the current because of the
12 settling out of the particles which in fact reduces the density difference. Their spatial
13 structure is determined mainly by their grain-size distribution flow behaviour is distinguished
14 depending on whether it is formed by fine or coarse grains), whereas their temporal
15 evolution is determined by both grain-size distribution and concentration (Felix, 2002).
16 Gladstone et al. (1998) found that the distance to which coarse particles are transported
17 within bi-disperse turbidity currents increases substantially as the proportion of fines in the
18 flow is increased, and that adding small amounts of fine sediment to a coarse-grained gravity
19 current has a much larger influence on flow speed, run-out distance and deposition patterns
20 than adding a small amount of coarse sediment to a fine-grained turbidity current.

21
22 Houtt (1972) and Fannelop & Waldman (1972) studied the specific problem of lock-release
23 oil slick and Chen (1980) studied spills of other hazardous fluids. Bonnecaze et al. (1993)
24 studied a particle-laden gravity current of finite volume spreading over a rigid un-obstructed
25 horizontal surface, assuming that particles diluted were non-cohesive and monodisperse
26 with equal settling velocity; they applied shallow-water equations that led to a relationship
27 between the length of the particle-driven current, x_c , and time since release, t , that was found
28 to be $x_c \sim t^{2/3}$.

1
2
3
4
5
6
7
8
9
10
11
12
13
14
15
16
17
18
19
20
21
22
23
24
25
26
27
28

When turbidity currents encounter arrays of obstacles, such as vegetation canopies in saltmarshes, lake littoral zones and seagrass meadows, the obstacles' drag forces act to reduce the currents' speed, as well as causing decreases in bed shear stress, which lead to reduced erosion and transport of bed sediment (Zong and Nepf 2011; Montakhab et al., 2012). However, work on turbidity currents' interactions with vegetated canopies and other arrays of obstacles has so far been restricted to understanding their hydrodynamics. As a result, the influence of these interactions on the currents' sediment transport and deposition is currently poorly understood. Recently, Testik and Yilmaz (2015) have studied the propagation of continuous-flux release gravity currents through emergent vegetation but experiments were conducted with non-Newtonian mud gravity currents. To our knowledge, the novelty of this study is the fact that it has studied the effect of emergent vegetation on a gravity current driven by the presence of suspended particles, and not generated by a saline dissolution. This paper, therefore, sets out to investigate the influences of characteristics of both turbidity currents and arrays of obstacles through which they flow on their hydrodynamic and sedimentary development

METHODOLOGY

Experiments were conducted in a 4 m long, 0.3 m high and 0.3 m wide methacrylate flume (Fig. 1) that was separated into two sections by a removable vertical lock gate: the shorter section (to the left in Fig. 1A) acted as a reservoir in which the sediment-laden water that would form the turbidity current was prepared, while the longer section (to the right in Fig. 1A) formed the experimental section in which the interaction of the turbidity current with the array of obstacles occurred. The experimental section was populated with vertical PVC dowels intended as generic models of the rigid stems of plants in an emergent vegetation

1 canopy. Hereinafter, we use the term “canopy” to refer to this array of dowels, and in doing
2 so implicitly acknowledge that they are an artificial, generic model of a vegetation canopy.
3 This experimental configuration can also be taken to represent a generic model of a much
4 wider range of interactions of turbidity currents with arrays of isolated, rigid obstacles, for
5 example, the propagation of snow avalanches or pyroclastic flow through forests, or of
6 submarine turbidity currents on continental shelves through offshore wind turbine farms.
7 The dowels’ positions were selected by means of a random number generator, following
8 Pujol et al. (2013). Each dowel had a height of 20 cm and a diameter, $d = 0.6$ cm, and was
9 inserted into a perforated PVC base sheet. The canopy density was quantified, following
10 Pujol et al. (2010) using the Solid Plant Fraction (SPF), which is defined as the fractional
11 area at the bed occupied by the dowels, $SPF = 100N\pi(d/2)^2/A$, where N is the number of
12 plants and A is the total bed area. In the present study, in addition to cases where no canopy
13 was present ($SPF = 0\%$), two canopy densities were used. These had SPF of 1% and
14 2.5%, which correspond to 128 and 320 obstacles m^{-2} , and values of the frontal area of
15 obstacles per unit volume of 0.02 to 0.05 cm^{-1} , respectively (Fig. 1B). These correspond to
16 dimensionless array densities ad of 0.01 and 0.03, which fall within the range observed in
17 natural vegetation canopies (e.g. $ad = 0.01$ to 0.1, Kadlec, 1990).

18

19 The flume was filled with water to a height $H = 12$ cm, and the lock gate put in place, sealing
20 off the two sections from each other. A volume of 3 litres of water was taken from the
21 reservoir section, to which sediment was added, stirring vigorously for five minutes to ensure
22 full mixture of the particle suspension. The sediment-laden water sample was then returned
23 to the reservoir section and mixed with the remainder of the water therein, giving an initial
24 sediment concentration, C_0 . Five values of C_0 – 1, 2.5, 5, 7.5, and 10 gL^{-1} – were used. The
25 sediment was taken from four field sites in the Empordà Marshes Natural Park, located in
26 the North-East of Spain, and was a mixture of clays, silts and very fine sands. Its particle
27 size distribution was determined using a LISST-100 particle size analyser (Sequoia

1 Scientific, Inc., WA, USA). This instrument determines the volume occupied by particles in
2 each of 32 size classes logarithmically distributed in the range of 2.5–500 μm . The size
3 distribution was found to be bimodal, with 80% of the mass made up of coarse particles
4 (diameter range: 6.2–104 μm) and the remaining 20% made up of fine particles (diameter
5 range: 2.2–6.2 μm). Based on the classifications of Van Rijn (2007) and Blott and Pye
6 (2012), the coarse particles fell into the category of weakly cohesive particles (fine to coarse
7 silts and small sand particles), and the fine particles into the category of very cohesive
8 particles (clays and very fine silts) (Fig. 2). The peak in Fig. 2 above 104 μm was assumed
9 to represent just a few particles with large volumes, which, due to their small number, were
10 not considered in the analysis.

11

12 Once the suspended sediment was well-mixed into the water in the reservoir, and the
13 turbulence caused by this mixing had decayed, the lock gate was lifted to release the
14 sediment-laden water, which flowed into the experimental section as a turbidity current.
15 Speeds of experimental currents were of 2-3 orders of magnitude higher than settling
16 velocity of coarse particles, and of 3-4 orders of magnitude higher than settling velocities of
17 fine particles being therefore sufficiently high to suspend the particles in a well-mixed state.
18 Thirteen sediment traps (ST1 to ST13), with volumes of 21.3 mL each, were placed on the
19 bottom of the experimental flume section at 20 cm intervals, starting 20 cm from the lock
20 gate (Fig. 1A) and finishing at 10 cm the end of the flume. These collected sediment
21 deposited from the turbidity current as it proceeded along the flume. When the current
22 arrived at the far end of the canopy, the traps were covered with lids to avoid collection of
23 sediment that settled out of the current after it had been reflected by the end wall. They
24 were then collected for size distribution analysis using the LISST-100. By integrating across
25 all of the particle size classes, the total volume of particles in each trap was obtained (Serra
26 et al. 2002b, 2005). This was then transformed into deposited sediment mass assuming that
27 the density of the particles was $2.798 \text{ g}\cdot\text{cm}^{-3}$ (the standard value for the density of silt
28 particles, Mandal and Maiti, 2015). This density is used because 80% of the sediment

1 volume was made up of silt particles (Figure 2). The deposited mass per unit bed area was
2 converted to a depositional flux rate at each sediment trap by dividing by the time over which
3 the deposition occurred. Five turbidity sensors, T1 to T5, (Seapoint Turbidity Meter, Seapoint
4 Sensors Inc., NH, USA) and two CCD cameras mounted on stationary tripods over the tank
5 (Fig. 1A), were used to measure the time evolution of the current's front and determine its
6 speed. This was done in two ways: firstly, by dividing the distance between pairs of turbidity
7 sensors by the difference in the time taken for the front to reach them, and secondly from the
8 images captured by the CCD cameras. The front's position was located on these images
9 using edge detection. Parallax error was less than 4% in these images and was not
10 corrected for in the analysis. Variations of 2% were found between velocity values calculated
11 from the turbidity sensor data and the camera images.

12

13 Fifteen experimental runs were carried out (Table 1), covering the full matrix of combinations
14 of five values of initial sediment concentration, C_o , (1, 2.5, 5, 7.5, and 10 gL^{-1}) and three
15 different canopy densities (SPF values of 0, 1 and 2.5%).

16

17 RESULTS

18

19 *Advance of the turbidity current*

20

21 The progression of the leading edge – or “toe” as it is called by Tanino et al. (2005) – of the
22 turbidity current was analysed. In non-vegetated experiments, its distance from the lock
23 gate, x_{toe} , was plotted against time (t) for the five experimental runs (Fig. 3A). For all
24 sediment concentrations x_{toe} presents a power trend. . At later times the loss of particles
25 reduced the buoyancy force driving the current, causing deviations from $x_{\text{toe}} \propto t$. This
26 behaviour can be also found in cases where $\text{SPF} \neq 0$ (Fig 3B, 3C) for which the deviation is
27 more accentuated due to the effect of vegetation which also influences the current speed.

1
2 Gravity currents generated in not vegetated experiments flowed with a constant speed along
3 the whole flume following inertial regime, resulting in agreement with Rottman and Simpson
4 (1983) findings. In vegetated experiments (SPF 1% and 2.5%), although they were carried
5 out by an infinite release, the gravity current transitioned from the inertial to the drag-
6 dominated regime (as finite volume releases do). Presumably this is caused because
7 reflections from the back wall travel through un-obstructed fluid whereas the particle-driven
8 current is propagating through the obstacles resulting in a slowing down speed which
9 therefore can interact with the reflected bore... In order to elucidate the moment at which the
10 gravity currents in the vegetated cases changed from the inertial to the drag-dominated
11 regime, it was studied the temporal dependency of data from the SPF=1% and SPF=2.5%
12 runs. As can be seen in Figure 4A, at early times, the behaviour of the gravity currents
13 flowing through vegetation canopies had a $\sim t^{-1}$ dependency (Equation 3), in agreement with
14 the findings of Tanino et al. (2005), and similar to that of the gravity current in the non-
15 vegetated case, but once the drag effect of the vegetation became more significant, it
16 reduced current speed and it was found a dependency of the toe position with $t^{1/2}$ in
17 agreement with the findings of Hatcher et al. (2000). The point at which this change occurred
18 was used to deduce that the transition from the inertial to the drag dominated regime
19 occurred and it coincided with $C_D a x_{toe} = 5$ value (where C_D is the array drag coefficient, a the
20 frontal area of cylinders per unit volume and x_{toe} the current toe position along the flume).
21 Tanino et al. (2008) found that $C_D a L = 7$ (where L corresponds to x_{toe} in this manuscript). This
22 value is smaller than the one found by Tanino et al. (2008), implying that particle-driven
23 currents are affected by vegetation drag earlier than salinity-driven gravity currents. Data
24 which $C_D a x_{toe} \geq 5$ are plotted against $((q_0 \cdot g' \cdot d) / (C_D \cdot \phi))^{1/4} \cdot t^{1/2}$ (Equation (1) from Hatcher et al,
25 2000) (which incorporates the effect of sediment concentration – quantified as g' – and the
26 effect of the canopy – quantified via C_D and ϕ , although models salinity driven currents) in
27 Fig. 4B.

1

2 These agreements were found regardless of both the initial sediment concentration and the
3 canopy density because particle-driven currents behave similarly to saline ones before
4 appreciable settling occurs. In Figure 4B in the range of the x axis from 200 cm to the end of
5 the flume measurements slightly deviate from the general trend $t^{1/2}$ depending on the initial
6 sediment concentration. The model developed by Hatcher et al. (2000) corresponded to
7 salinity-driven gravity currents; therefore since particles were not included in the model, the
8 experimental results might slightly shift from those obtained by Hatcher et al. (2000). The
9 reason might be in the fact that laden gravity currents might lose sediment particles as they
10 travel along the flume. It is expected that this process has a greater effect for denser gravity
11 currents.

12 In addition, while the time dependence between x_{toe} and t is in accordance with that
13 predicted by both, Tanino et al. (2005) and Hatcher et al. (2000), depending of the regime, a
14 slower slope was found. In the inertial regime, our data follow a slope of 0.4 while a higher
15 slope of ~ 1 was found by Tanino et al. (2005). In the drag-dominated regime, our data follow
16 a slope of 0.7 while a higher slope of ~ 2 was found by Hatcher et al. (2000). This smaller
17 slope values are occasioned because the models which have been used to compare both
18 regimes ($x_{toe} \sim t$ and $x_{toe} \sim t^{1/2}$) corresponded to salinity-driven gravity current instead of being a
19 particle-laden current. Experiments developed with particle-driven currents change their
20 speed when settling occurs and also, it has to be in account the effect of particle capture
21 on the cylindrical stems (Palmer et al. 2004). This loss of sediment causes a reduction on
22 current speed happening therefore in a decreasing gradient, as found.

23

24 *Sediment transport and deposition*

25

26 Figure 5 presents the depositional flux rates for runs with an initial sediment concentration of
27 1 gL^{-1} at the thirteen sediment traps within the canopy. The not-vegetated cases (SPF = 0%)

1 show a clear difference between the depositional flux rates of the fine and coarse particle
2 fractions, with the fine fraction peaking approximately two-thirds of the way down the
3 canopy, while the flux of coarse particles decayed essentially monotonically with distance
4 from the lock gate. These patterns are similar to those found in experiments on bi-disperse
5 turbidity currents with the same initial proportions by mass as were used here – 80% coarse
6 particles and 20% fine particles – carried out by Gladstone et al. (1998). In those
7 experiments, the depositional density of the fine fraction reached its maximum value at a
8 position that was independent of the initial concentration of fines, and the coarse fraction
9 deposition was greatest nearest to the lock gate.

10

11 The plots of depositional flux rates in the runs where canopies are present (Fig. 5 B,C,E and
12 F) show the flow regimes through which the turbidity current develops: the initial, inertial
13 regime ($C_D a x_{toe} < 5$), and the drag-dominated regime ($C_D a x_{toe} \geq 5$). For experiments with the
14 presence of vegetation, only a ~62% (SPF 1%) and a ~38% (SPF 2.5%) of the sediment
15 from the gravity current penetrate within the canopy when compared with the not vegetated
16 experiment. Furthermore, the SPF = 1% canopy causes the depositional flux rates of fine
17 and coarse particles (Figs. 5B and 5E) to decay consistently from the lock gate through the
18 inertial regime, and to reach their minima at $L \approx 200$ cm. In the beginning of the drag-
19 dominated regime, these flux rates remain essentially constant, a slight increase at the end
20 of the flume is caused by the fact that deposit values at each sediment tramp (ST) have
21 been divided by the time over which the deposition occurred, for this reason last ST value
22 were removed because the elapsed time biased the data from the plot.. In the denser
23 canopy runs (SPF = 2.5%, Figs. 5C and 5F), flux rates remain essentially constant along the
24 flume. It can be also seen that the flux rates are higher here than for the corresponding SPF
25 = 1% cases, as the current is moving slower.

26

1 Fine and coarse sediment log depositional flux rates for all runs are plotted in Figs 6 and 7
2 respectively. Across all of these plots there is a consistent pattern of greater initial sediment
3 concentrations leading to larger depositional flux rates. The fine particles in the not-
4 vegetated (SPF = 0 %) runs with initial sediment concentrations of 1 and 2.5 gL⁻¹ (Fig. 6A)
5 had maximum depositional flux rates at x = 180 and 220 cm, respectively, while in
6 experiments with higher initial concentrations, the maximum fine particle depositional flux
7 rates are found at ST12, the furthest sediment trap from the lock gate (x = 240cm). For the
8 SPF = 1% and 2.5% cases (Figs. 6B and 6C, respectively), the fine particle depositional flux
9 rates for lower initial sediment concentrations (1 and 2.5 gL⁻¹) reached minima at runout
10 distances of x = 200 and 220 cm, while in the higher initial concentration cases (5, 7.5 and
11 10 gL⁻¹), these rates were constant up to the same point, and increased slightly thereafter. It
12 can also be seen that curves were gathered in two groups depending on their initial
13 concentration: low initial concentration (1, 2.5 g/l) and high initial concentration (5, 7.5, 10
14 g/l).

15 Depositional flux rates of coarse fraction sediments in not-vegetated runs (SPF = 0%) with
16 low initial sediment concentrations (1, 2.5 and 5 gL⁻¹) decreased with runout distance until x
17 = 200-220 cm (Fig. 7A). Runs with sediment concentrations of 7.5 and 10 gL⁻¹ had constant
18 coarse fraction depositional flux rates from x = 0 to 200 cm and increased thereafter. In runs
19 with vegetation (Fig. 7B and 7C), the coarse sediment depositional flux rates decreased with
20 runout distance until x = 200 cm in a similar fashion for all initial sediment concentrations. In
21 the SPF = 1% cases (Fig. 7B), differences in the depositional flux rates between low (1 and
22 2.5 gL⁻¹) and high (5, 7.5 and 10 gL⁻¹) initial sediment concentrations were more
23 accentuated. As seen before with fine sediments, curves were also gathered in two groups
24 depending on their initial concentration: low initial concentration (1, 2.5 g/l) and high initial
25 concentration (5, 7.5, 10 g/l). As shown in Fig. 8, the amount of coarse particles in the
26 deposited sediments diminished along the flume. The amount of fine particle deposition was
27 maximum at ST12, the sediment tramp located at x = 240cm, (corresponding to C_Dαx_{toe}
28 values of 12 (for sediment concentration 5 gL⁻¹, SPF 1%) and 42 (for sediment concentration

1 2.5 gL⁻¹, SPF 2.5%). At this point, and for an initial sediment concentration of 5 gL⁻¹,
 2 regardless of the canopy density (Fig. 8C and 8D) both the fine fraction and the coarse
 3 fraction were found in larger concentrations than at traps further upstream. This supports the
 4 theory that finer particles increase the distance to which coarser particles are transported, in
 5 agreement with the findings of Gladstone et al. (1998).

6

7

8 DISCUSSION

9

10 Our results demonstrate that when turbidity currents develop in an array of isolated, rigid
 11 obstacles (intended here to simulate vegetation canopies), the patterns of deposited
 12 sediment depend on whether the current is in an inertia-dominated regime or a drag-
 13 dominated regime. For each canopy density, a drag coefficient may be calculated and used
 14 to quantify the array drag $C_D a x_{toe}$ at each downstream location, x_{toe} , of the gravity current
 15 front. This defines the regime of the flow, and conveniently classifies it (Hogg and Woods et
 16 al. 2001; Tanino et al. 2005) and thus its depositional flux rates.

17

18 *Gravity flow characteristics within a canopy*

19

20 In Tanino et al.'s (2005) data, if $C_D a L < 7$, the gravity current was inertia-dominated, whereas
 21 if $C_D a L > 7$ it transitioned to a drag-dominated regime, being fully drag dominated if $C_D a L > 18$.

22 In our study, where a particle-driven gravity current was studied instead of Tanino et al.'s
 23 salinity-driven gravity current, the $C_D a L (C_D a x_{toe})$ threshold value for the beginning of the
 24 transition from the inertial regime to the drag-dominated regime was $C_D a x_{toe} = 5$.

25 Analysis of frontal progression of gravity currents through arrays of obstacles in finite lock-
 26 release experiments shows that it in the initial inertial regime $x_{toe} \sim t$ and in the subsequent
 27 drag-dominated regime $x_{toe} \sim t^{1/2}$ (Tanino et al., 2005, Zhang and Nepf, 2008). Our results,
 28 although found in an infinite lock-release set up, show the same behaviour. As the gravity

1 current is initiated just before the canopy starts, the volume fraction of solid that current has
2 to face is so high that the gravity current flows slower than it would, allowing the bore,
3 generated in the back wall, to catch up with the front. At this moment the flow transitions to a
4 drag-dominated regime $x_{toe} \sim t^{1/2}$ in agreement with Hatcher et al. (2000). The differences in
5 the slope (proportionality constant) between our results and those of Tanino et al. (2005) and
6 Hatcher et al. (2000) mentioned above may be due to the characteristics of density-varying
7 agent within the current and vegetation set up. While Tanino et al. (2005) and Hatcher et al.
8 (2000) used a salinity-driven current, our experiments have been with a particle-driven
9 current. Again, the loss of particles settling out and by canopy capture caused a decrease of
10 its density and as a result a decrease of its speed. In summary, this study provides evidence
11 to support the theory that the dynamical balance between the array drag and the streamwise
12 pressure gradient (which is the basis of the predictions of Hatcher et al., 2000) provides a
13 good description of the propagation of a poly-disperse turbidity current for a finite-volume
14 release through an array of isolated, rigid obstacles. In addition, the vegetation distribution
15 along the flume differs from the Tanino et al. (2005) and Hatcher et al. (2000), starting just
16 after the lock gate, the sudden encounter with canopy causes a slower speed that current
17 would have compared with the whole flume covered with vegetation and in consequence a
18 lower value of the slope of the trend between x_{toe} and t in both the inertia and the drag-
19 dominated regime.

20

21

22 *Depositional sediment fluxes from the gravity current*

23

24 As pointed out by Felix (2002), sediment concentration and velocity can influence flow
25 behaviour independently. Within an array of isolated obstacles, such as a vegetation canopy,
26 the obstacles' presence may induce momentum loss due to both, or either, decreasing
27 velocity (due to their drag) and decreasing density (due to sediment deposition), and these
28 two mechanisms need not to occur at the same time because the different time scales on

1 which they take place. In our experiment, variations in sediment concentration (and its rate
2 of decrease due to deposition) and frontal speed were both primarily determined by whether
3 the current was in an inertia-dominated or drag-dominated regime. In the inertia-dominated
4 regime, the speed of propagation was slightly diminished and the depositional flux rate of the
5 sediment decreased with time. In the drag-dominated regime, the speed of propagation
6 decreased with time more quickly, and the depositional flux rate of the sediment increased
7 with time.

8

9 Bonneau et al. (1996) and Harris et al. (2002), found that smaller particles are more easily
10 transported than large particles, and that this causes the magnitude and downstream
11 position of the depositional maximum to be greater for small particles. This occurs because
12 while the coarse particles settle out, the fine particles remain in suspension and thus
13 maintain the density difference between the current and the ambient. This was clearly
14 observed in our experiments for the lowest initial sediment concentration (1 gL^{-1}) in the
15 absence of a canopy, while at high particle concentrations, the depositional rate of both the
16 fine and coarse particle fractions was still rising when the current front reached the end of
17 the flume.

18

19 From the results of all of our runs, the depositional flux rate was found to depend on the
20 canopy density, and the initial sediment concentration of the current, and to differ depending
21 on whether the fine or coarse particle size fraction was being considered. These
22 dependencies are summarised in Fig. 9 where it is plotted the depositional flux rate,
23 normalized by the initial advective (horizontal) sediment flux at the lock gate (calculated by
24 multiplying initial sediment concentration by initial current speed). This dimensionless flux
25 rate decreased with $C_{Dax_{toe}}$ for both the fine (Fig. 9A, B) and coarse (Fig. 9C, D) fractions
26 when the gravity current was in the inertial-dominated regime, whereas it increased at the
27 end of the drag-dominated regime. This was found for all runs except for the fine fraction in

1 the cases where the initial sediment concentration was high (10gL^{-1}) and the canopy density
2 was low (SPF = 1%), in which the rate increased through the inertia-dominated regime.

3

4 For lower canopy density (SPF = 1%), the dimensionless normalised depositional flux rates
5 for both size fractions is stratified, decreasing gradually with decreasing initial concentration
6 (Fig. 9A and 9B). The same overall trend was found for the denser canopies (SPF = 2.5%),
7 but the data splits into two clear groups: for both particle size fractions, dimensionless
8 normalised depositional flux rates for the larger initial sediment concentrations (5, 7.5 and 10
9 gL^{-1}) are approximately one order of magnitude larger than those for the smaller initial
10 sediment concentrations (1 and 2.5 gL^{-1}). It has been found that that this distinction occurs
11 whether the C_D is larger or lower than 2. Therefore, denser canopies act to segregate
12 sediment pattern from the gravity current, depending on its initial sediment concentration,
13 whether the C_D is larger or lower than 2.

14 In the SPF = 1% cases, the dimensionless normalised depositional flux rates reached
15 minima and began to increase in the beginning of the drag-dominated zone ($5 < C_{D\text{max}_{\text{toe}}}$),
16 while for the SPF = 2.5% cases, this occurred only when the current reached the end of the
17 drag-dominated regime. Thus, for both the fine and coarse fractions, maximal dimensionless
18 normalised depositional flux rates occurred in the drag-dominated regime. The increase in
19 depositional flux rates at this relatively late stage implies that the currents are able to retain
20 much of their suspended material until they become significantly impeded by the drag of the
21 canopy. The ratio of the current's advective speed to the particles' fall speed in the inertia-
22 dominated regime is 955 for particles of 4 μm diameter and 375 for particles of 20 μm
23 diameter (where fall speed was calculated assuming Stokes' Law) and in the drag-
24 dominated regime is of 128 for particles of 4 μm diameter and 50 for particles of 20 μm
25 diameter, indicating the dominance of advective processes in the inertial regime. This
26 dominance is likely to be enhanced by the action of the vertical turbulent component of
27 velocity within the current, which helps to maintain the particles in suspension. This effect is

1 likely to be greater in the inertial regime than in the drag-dominated regime, since the ratio of
 2 the cylinder Reynolds number associated to the front (toe) of the current in the inertial
 3 regime to that in the drag-dominated regime is 2-4.

4 In summary, the propagation of particle-driven gravity currents, and the patterns of
 5 deposition that they create which are reported here were found to be functions of canopy
 6 density, suspended sediment characteristics (sediment concentration and grain size) and
 7 distance from the current's source. The evolution of the currents and their depositional
 8 patterns may be categorised into an early, inertia-dominated stage in which deposition rates
 9 mainly decrease monotonically, and a late drag-dominated stage, in which deposition rates
 10 tend to peak. These stages are effectively delineated, by values of the array drag term
 11 $C_{Dax_{toe}} < 5$ (inertia -dominated) and >5 (drag dominated), which are close, but not identical,
 12 to those reported for salinity-driven gravity currents by Tanino et al. (2005).

13 Canopies act on gravity currents in first place allowing only a part of particles to flow into,
 14 therefore, the presence of canopies not only play an important role in the sediment
 15 deposition within the canopy but also in regions before the canopy, where a great amount of
 16 sediment is deposited compared without the presence of vegetation. Once inside, coarse
 17 particles settle monotonically from the first moment while finer particles run further from the
 18 beginning of the canopy. Then a sediment gradation depending on distance from the canopy
 19 edge is found, being located the coarse sediments (fine to coarse silts and small sand
 20 particles) near the edge while finer sediments (clays and very fine silts) are located at further
 21 distances.

22

23 NOMENCLATURE

24

25 a, frontal area of the cylinders per unit volume

26 a_d , dimensionless array density

27 c_o , initial sediment concentration

28 C_D , Drag coefficient

- 1 d, dowel diameter
- 2 ϕ , vegetation volume fraction
- 3 g' , reduced gravity based on the density difference between the two layers
- 4 H, height of water
- 5 L, distance of the turbidity current front from the lockgate ($L=x_{toe}$) used in Tanino et al. (2005)
- 6 n, vegetation porosity
- 7 PVC, particle volume concentration
- 8 q_o , total current volume per unit across-flume distance
- 9 Re , flow Reynolds number
- 10 Re_c , cylinder Reynolds number
- 11 SPF, fractional plant area at the bottom occupied by stems
- 12 x_{toe} , distance of the turbidity current front from the lockgate
- 13 u, instantaneous current front velocity
- 14

15 REFERENCES

16

17 **Adduce C., Sciortino G. and Proietti S.** (2012) Gravity currents produced by lock-
18 exchanges: experiments and simulations with a two layer shallow-water model with
19 entrainment. *Journal of Hydraulic Engineering*, **138(2)**, 111-121

20

21 **Benjamin, T. B.** (1968) Gravity currents and related phenomena. *J. Fluid Mech.*, **31**, 209–
22 248.

23

24 **Bhaganagar, K.** (2014) Direct numerical simulation of lock-exchange density currents over
25 the rough wall in slumping phase. *Journal of Hydraulic Research*, **52(3)**, 386-398

26

27 **Bonnecaze, R.T., Huppert, H.E. and Lister, J.R.** (1993) Particle-driven gravity currents. *J.*
28 *Fluid Mech.*, **250**, 339-369

1
2
3
4
5
6
7
8
9
10
11
12
13
14
15
16
17
18
19
20
21
22
23
24
25
26
27
28

Bonnecaze, R.T., Huppert, H.E. and Lister, J.R. (1996) Patterns of sedimentation from polydispersed turbidity currents. *Proc. R. Soc. Lond. A*, **452**, 2247-2261

Blott, S.J. and Pye, K. (2012) Particle size scales and classification of sediment types based on particle distributions: review and recommended procedures. *Sedimentology* **59**, 2071–2096.

Burke, R. W., and Stolzenbach, K. D. (1983) Free surface flow through salt marsh grass, MIT Sea Grant Coll. Program Rep. MITSG 83-16, Massachusetts Institute of Technology, Cambridge.

Chen, J-C. (1980) Studies on gravitational spreading currents, Thesis. Caltech University.

Chikita, K. (1989) A field study on turbidity currents initiated from spring runoffs. *Water Resources Research*, **25**, 257-271.

Fannelop, T.K. and Waldman, G.D. (1972) Dynamics of oil slicks. *AIAA J.* **10**, 506-510.

Felix, M. (2002).Flow structure of turbidity currents. *Sedimentology*, **49**, 397-419.

Gladstone, C., Phillips, J.C. and Sparks, R.S.J. (1998) Experiments on bidisperse, constant-volume gravity currents: propagation and sediment deposition. *Sedimentology*, **45**, 833-843.

Gonzalez-Juez, E., Meiburg, E. and Constantinescu, G. (2009) Gravity current mixing in gravity currents propagating up mild slopes flow past a circular cylinder: flow fields and associated forces. *J. Fluid Mech.* **631**, 65-102

1
2
3
4
5
6
7
8
9
10
11
12
13
14
15
16
17
18
19
20
21
22
23
24
25
26
27
28

Gonzalez-Juez, E., Meiburg, E., Tokyay, T. and Constantinescu, G. (2010) Gravity current mixing in gravity currents propagating up mild slopes flow past a circular cylinder: forces, wall shear stresses and implications for scour. *J. Fluid Mech.* **649**, 69-102

Hatcher, L., Hogg, A.J. and Woods, A.W. (2000) The effect of drag on turbulent gravity currents. *J. Fluid Mech.*, **416**, 297-314.

Harris, T.C., Hogg, A.J. and Huppert, H.E. (2002) Polydisperse particle-driven gravity currents. *J. Fluid Mech.*, **472**, 333-371.

Honeyman, B. D. and Santschi, P. H. (1989) A Brownian-pumping model for oceanic trace metal scavenging: Evidence from Th isotopes. *Journal of Marine Research*, **47** (4), 951-992

Hogg, A.J. and Woods, A.W. (2001). The transition from inertia- to bottom-drag-dominated motion of turbulent gravity currents. *J. Fluid Mech.*, **449**, 201-224.

Hout, D.P. 1972 Oil spreading on the sea. *Ann. Rev. Fluid Mech.* **169**, 337-351.

Kadlec, R. H. (1990) Overland flow in wetlands: Vegetation resistance, *J. Hydraul. Eng.*, **116**(5), 691– 706.

Kneller, B. and Buckee, C. (2000) The structure and fluid mechanics of turbidity currents: a review of some recent studies and their geological implications, *Sedimentology*, **47**, 62-94.

La Rocca, M., Adduce, C., Sciortino, G. and Pinzon, A.B. (2008) Experimental and numerical simulation of three-dimensional gravity currents on smooth and rough bottom, *Phys. Fluids*, **20**(10), 106603(2008); doi:10.1063/1.3002381

1
2
3
4
5
6
7
8
9
10
11
12
13
14
15
16
17
18
19
20
21
22
23
24
25
26
27
28

Li, X. and Logan, B. E. (1997) Collision Frequencies of Fractal Aggregates with Small Particles by Differential Sedimentation. *Environ. Sci. Technol.* **31**, 1229 - 1236

Mandal, S. and Maiti, R. (2014) Semi-quantitative Approaches for Landslide Assessment and Prediction. Springer Natural Hazards. Springer, Berlin 292pp

Marino, M.L.P., Thomas, L.P. and Linden, P. (2005) The front condition for gravity currents. *J. Fluid Mech.*, **536**, 49-78

Meiburg, E., and Kneller, B. (2010) Turbidity currents and their deposits. *Annu. Rev. Fluid Mech*, **42**, 135–56

Montakhab, A., Yusuf, B., Ghazali, A. H., and Mohamed, T. A. (2012) Flow and sediment transport in vegetated waterways: a review. *Rev Environ Sci Biotechnol*, **11**, 275–287

Nepf, H. M. (1999). Drag, turbulence, and diffusion in flow through emergent vegetation. *Water Resources Research*, **35**, 2, 479-489.

Nogueira, H.I.S., Adduce, C., Alves, E. and Franca, M.J. (2013) Analysis of lock-exchange gravity currents over smooth and rough beds. *J. Hydraul. Res.*, **51(4)**, 417-431

Nogueira, H.I.S., Adduce, C., Alves, E. and Franca, M.J. (2014) Dynamics of the head of gravity currents. *Environ. Fluid. Mech.*, **14**, 519-540

Ozan, A.Y., Constantinescu, G. and Hogg, A.J. (2015) Lock-exchange gravity currents propagating in a channel containing an array of obstacles, *J. Fluid Mech.*, **765**, 544-575

- 1 **Palmer, M.R., Nepf, H.M., Petterson, T.J.R. and Ackerman, J.D.** (2004) Observations of
2 particle capture on a cylindrical collector: Implications for particle accumulation and removal
3 in aquatic systems, *Limnol. Oceanogr.*, **49(1)**, 76-85
4
5
- 6 **Pujol, D., Colomer, J., Serra, T. and Casamitjana, X.** (2010) Effect of submerged aquatic
7 vegetation on turbulence induced by an oscillating grid. *Continental Shelf Research*, **30**,
8 1019-1029.
9
- 10 **Pujol, D., Serra, T., Colomer, J. and Casamitjana, X.** (2013) Flow structure in canopy
11 models dominated by progressive waves. *Journal of Hydrology*, **486**, 281-292.
12
- 13 **Roget, E. and Colomer, J.** (1996). Flow characteristics of a gravity current induced by
14 differential cooling in a small lake. *Aquatic Sciences*, 58/4, 367-377.
15
- 16 **Serra, T., Colomer, J., Gacia, E., Soler, M. and Casamitjana, X.** (2002a).
17 Effect of a turbid hydrothermal plume on the sedimentation rates in a karstic lake.
18 *Geophysical Research Letters*, **29** (21), DOI 10.1029/2002 GL015368.
19
- 20 **Serra, T., Casamitjana, X., Colomer, J. and Granata, T.C.** (2002b) Observations of the
21 particle size distribution and concentration in a coastal system using an in situ laser
22 analyzer. *Marine Technology Society Journal* **36**, 59-69.
23
- 24 **Serra, T., Colomer, J., Julià, R., Soler, M. and Casamitjana, X.** (2005) Behaviour and
25 dynamics of a hydrothermal plume in lake Banyoles, Catalonia, NE Spain. *Sedimentology*
26 **52**, 795–808.
27

- 1 **Shin, J. O., Dalziel, S. B. and Linden, P. F.** (2004) Gravity currents produced by lock
2 exchange. *J. Fluid Mech.*, **521**, 1–34. DOI: 10.1017/S002211200400165X
3
- 4 **Simpson, J.E.** (1982) Gravity currents in the the laboratory, atmosphere, and ocean. *Annu.*
5 *Rev. Fluid Mech.*, 14, 213-234.
6
- 7 **Soler, M., Serra, T., Casamitjana, X. and Colomer J.** (2009) High sedimentation rates in a
8 karstic lake associated with hydrothermal turbid plumes (Lake Banyoles, Catalonia, NE
9 Spain). *Sedimentary Geology*, **222**, 5-15.
10
- 11 **Tanino, Y., Nepf, H.M. and Kulis, P.S.** (2005) Gravity currents in aquatic canopies. *Water*
12 *Resources Research*, **41**, W12402, doi: 10.1029/2005WR004216.
13
- 14 **Testik, F. Y. and Yilmaz, N. A.** (2015) Anatomy and propagation dynamics of continuous-
15 flux release bottom gravity currents through emergent aquatic vegetation. *Physics of Fluids.*,
16 **27**, 5, 1.4919783
17
- 18 **Van Rijn, L.C.** (2007) Unified view of sediment transport by currents and waves I: Initiation
19 of motion, bed roughness, and bed-load transport. *J. Hydraul. Eng.***133**, 649–667.
20
- 21 **White, F.M.** (1991) *Viscous Fluids Flow*, 2nd ed., McGraw-Hill, New York.
22
- 23 **Zhang X. and Nepf, H.M.** (2008) Density-driven exchange flow between open water and
24 aquatic canopy. *Water Resour. Res.*, **44**, W08417, doi:10.1029/2007WR006676
25
- 26 **Zhang X. and Nepf, H.M.** (2011) Exchange flow beteen open water and floating vegetation.
27 *Environ. Fluid Mech.*, **11(5)**, 531-546
28

1 **Zong, L. and H. Nepf** (2011) Vortex development behind a finite porous obstruction in a
2 channel, *Journal of Fluid Mechanics*, doi: 10.1017/jfm.2011.479.

3

4

5 CAPTIONS TO TABLES

6 Table 1. Summary of Experimental Conditions and parameters.

7

8 CAPTIONS TO FIGURES

9 Figure 1. (A) Side view of the laboratory flume which is divided by a removable, sealing
10 partition (lock gate) into two reservoirs. The smaller, lefthand one is filled with water to a
11 depth $H=12\text{cm}$ and suspended sediments of an initial concentration, C_0 . The righthand one
12 contains a random array of emergent cylindrical obstacles (PVC dowels, representing rigid
13 vegetation), and is filled with water to the same depth, H . The vertical coordinate is z , with
14 $z=0$ at the bed (increasing upwards), and the longitudinal coordinate is x , with $x=0$ at the lock
15 gate (increasing to the right). The vertical dashed lines indicate the position of five turbidity
16 sensors (T1–T5). Thirteen sediment traps (ST1-ST13) are situated on the bed of the flume;
17 ST1 is 20 cm to the right of the lock gate, and each subsequent trap is a further 20cm to the
18 right. (B) Dowels' horizontal positions generated to have a canopy randomly distributed with
19 a SPF of 1 and 2.5 %.

20

21 Figure 2. The bimodal particle size distribution (particle volume concentration, PVC, plotted
22 against particle diameter, d) of the natural sediments used for generating the gravity
23 currents. The distribution splits into fine particle (F.P: $2.5 \mu\text{m} < \phi < 6.2 \mu\text{m}$) and coarse
24 particle (C.P: $6.2 \mu\text{m} < \phi < 104.0 \mu\text{m}$) fractions.

25

1 Figure 3 Temporal evolution of the front of the turbidity current for runs with array densities
2 of (A) Not-vegetated; (B) SPF = 1 and (C) SPF = 2.5%.

3

4 Figure 4. Temporal variation of the length of the turbidity current for runs within array
5 densities of SPF=1% and SPF = 2.5%. (A) The dashed line illustrates the time dependence
6 predicted for inertial dominated conditions ($m= 0.4$, $r^2=0.93$, $n=47$, $p<<0.01$). (B) The dashed
7 line illustrates the time dependence predicted for drag dominated conditions ($m=0.7$, $r^2=0.94$,
8 $n=82$, $p<<0.01$).

9

10 Figure 5. Depositional flux rates plotted against distance from lock gate for experiments with
11 an initial concentration $C_0= 1\text{gL}^{-1}$. The lefthand panels (A, B and C) show results for the fine
12 particle fraction for SPF = 0 (Not-vegetated) 1 and 2.5% respectively. The righthand panels
13 (D, E and F) show corresponding results for the coarse particle fraction. For runs where an
14 array of obstacles is present i.e. $\text{SPF} \neq 0$ (B, C, E and F), the white areas correspond to the
15 quadratic drag-dominated regime ($C_{Dax_{toe}} < 5$) and the grey zones correspond to the linear
16 drag-dominated regime ($C_{Dax_{toe}} > 5$).

17

18 Figure 6. Semi-logarithmic plot of the depositional flux rate against distance for the fine
19 particle fraction (particle diameters $< 6.2 \mu\text{m}$) for different initial sediment concentrations (1,
20 2.5, 5, 7.5 and 10gL^{-1}). The panels show results for runs with (A) Not-vegetated; (B) SPF =
21 1%; and (C) SPF = 2.5% canopies.

22

23 Figure 7. Semi-logarithmic plot of the depositional flux rate against distance for the coarse
24 particle fraction (particle diameters $6.2 - 104 \mu\text{m}$) for different initial sediment concentrations
25 (1, 2.5, 5, 7.5 and 10gL^{-1}). The panels show results for runs with (A) Not-vegetated; (B) SPF
26 = 1%; and (C) SPF = 2.5% canopies.

27

1 Figure 8. Depositional flux rates plotted against particle diameter for 4 sediment traps (ST1,
2 ST4, ST7 and ST12) from runs with: (A) $C_0 = 2.5 \text{ gL}^{-1}$ and $\text{SPF} = 1\%$, (B) $C_0 = 2.5 \text{ gL}^{-1}$ and
3 $\text{SPF} = 2.5\%$, (C) $C_0 = 5 \text{ gL}^{-1}$ and $\text{SPF} = 1\%$, and (D) $C_0 = 5 \text{ gL}^{-1}$ and $\text{SPF} = 2.5\%$.

4

5

6 Figure 9. Dimensionless depositional flux rates (normalised by the initial depositional flux
7 rate - calculated by multiplying initial sediment concentration by initial current speed) plotted
8 against the array drag, $C_D a x_{toe}$. Panels A and C correspond to sparse canopy and B and D to
9 denser canopy. The white zone corresponds to inertial-dominated regime ($C_D a x_{toe} < 5$) and
10 the grey zone to the drag-dominated regime ($C_D a x_{toe} > 5$).

11 |

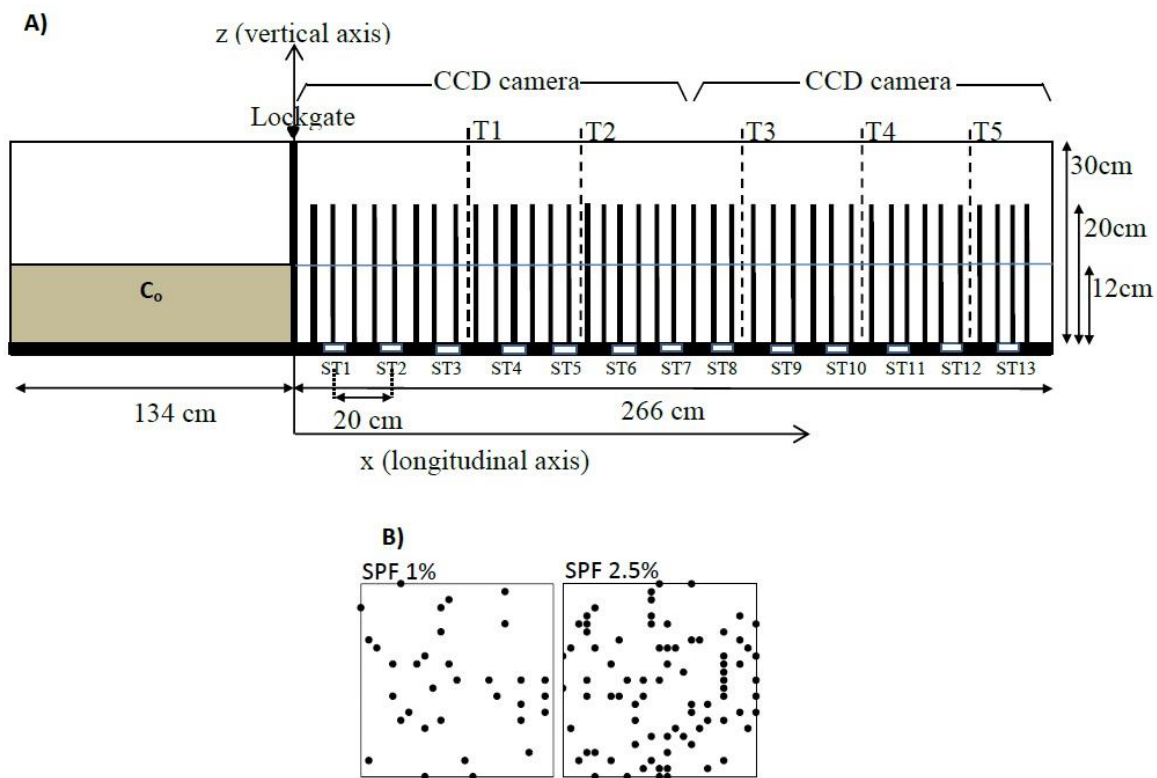


Fig. 1

1

2

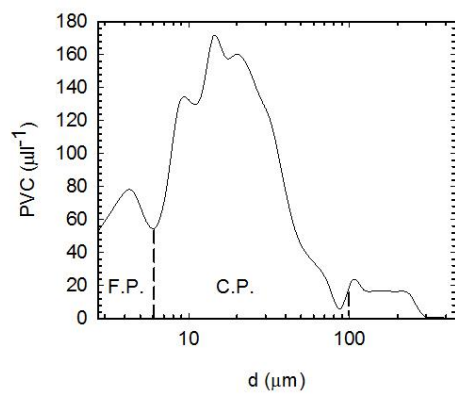


Fig. 2

1

2

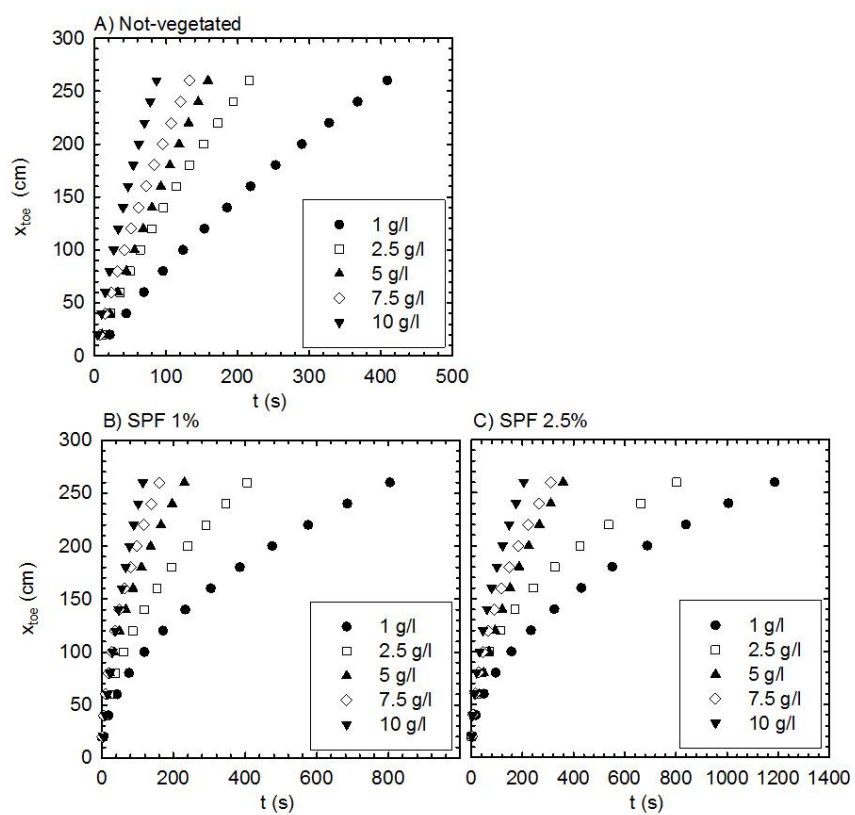


Fig. 3

1

2

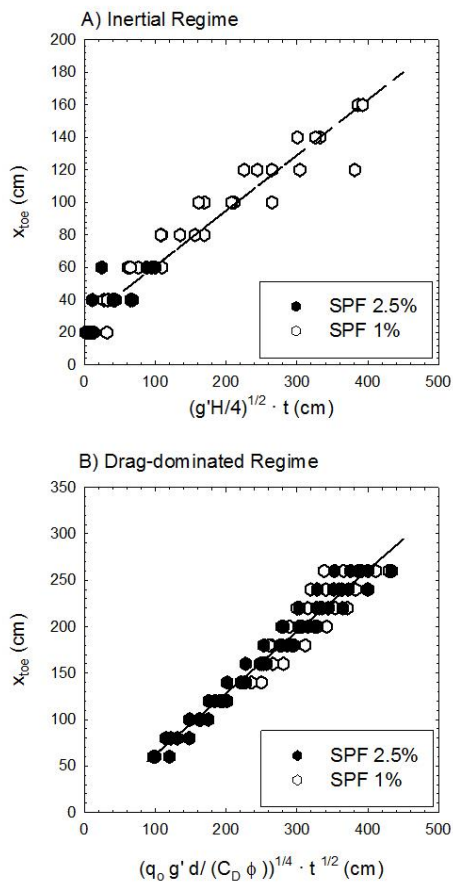


Fig. 4

1

2

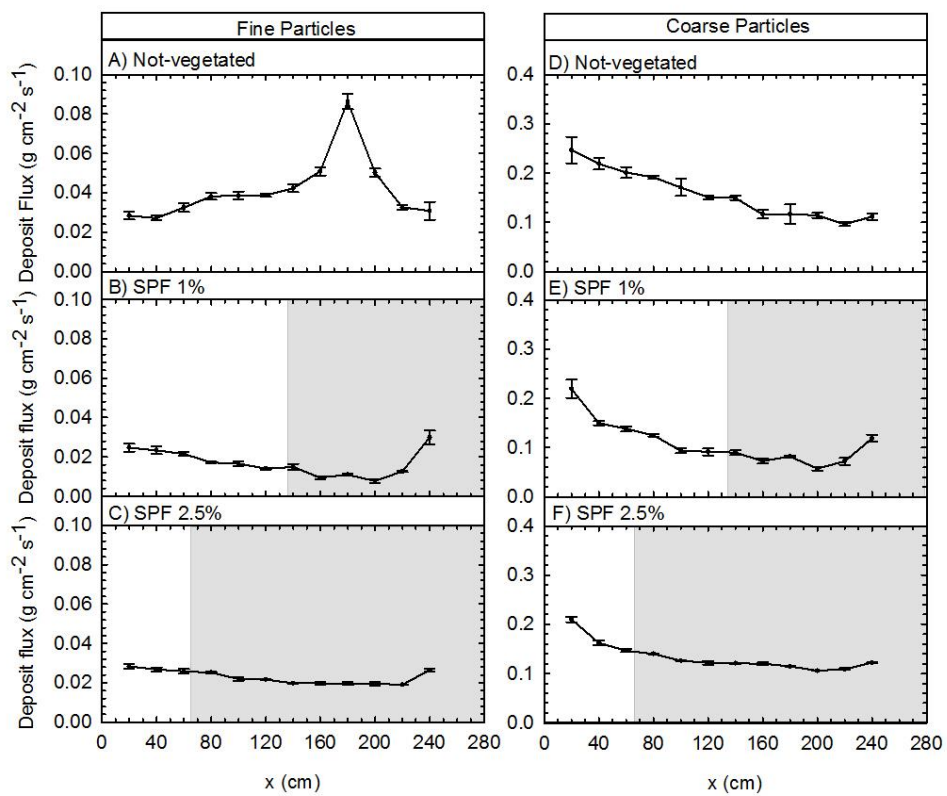


Fig. 5

1

2

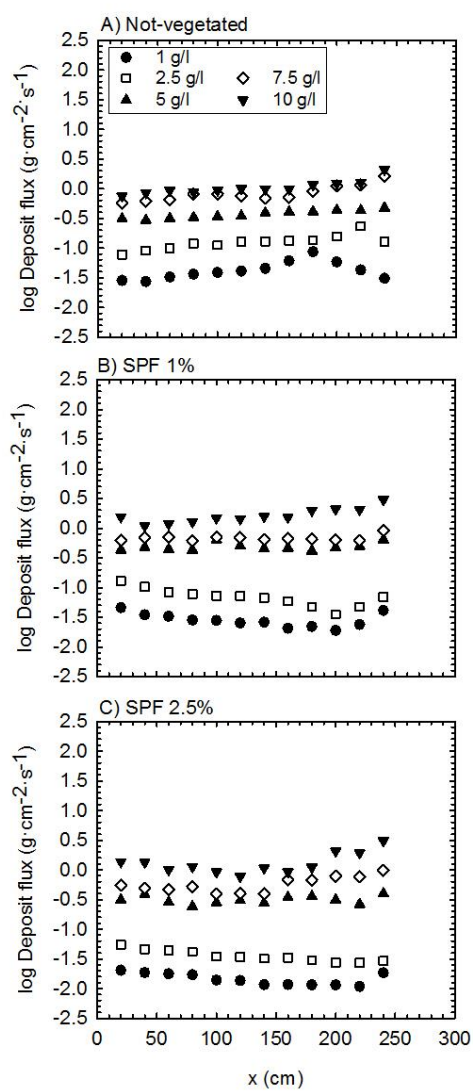


Fig. 6

1

2

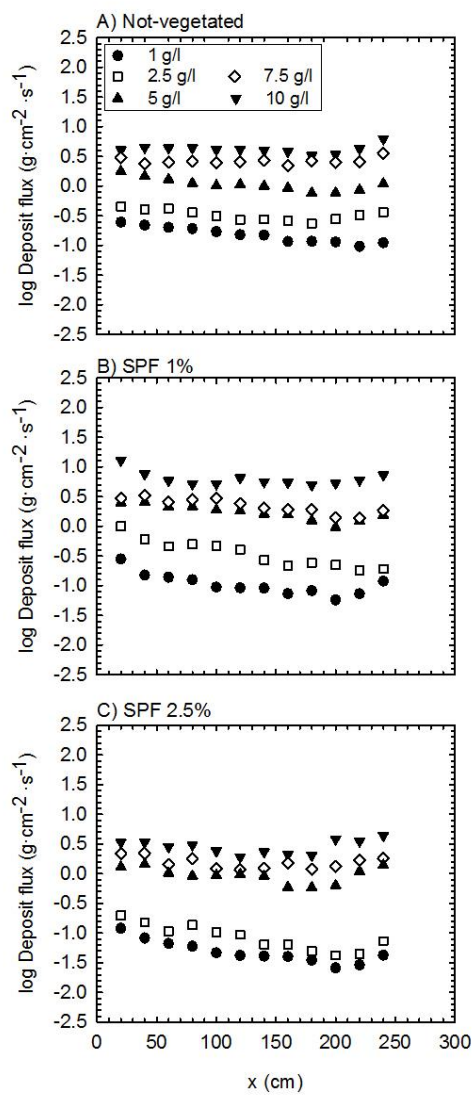


Fig. 7

1

2

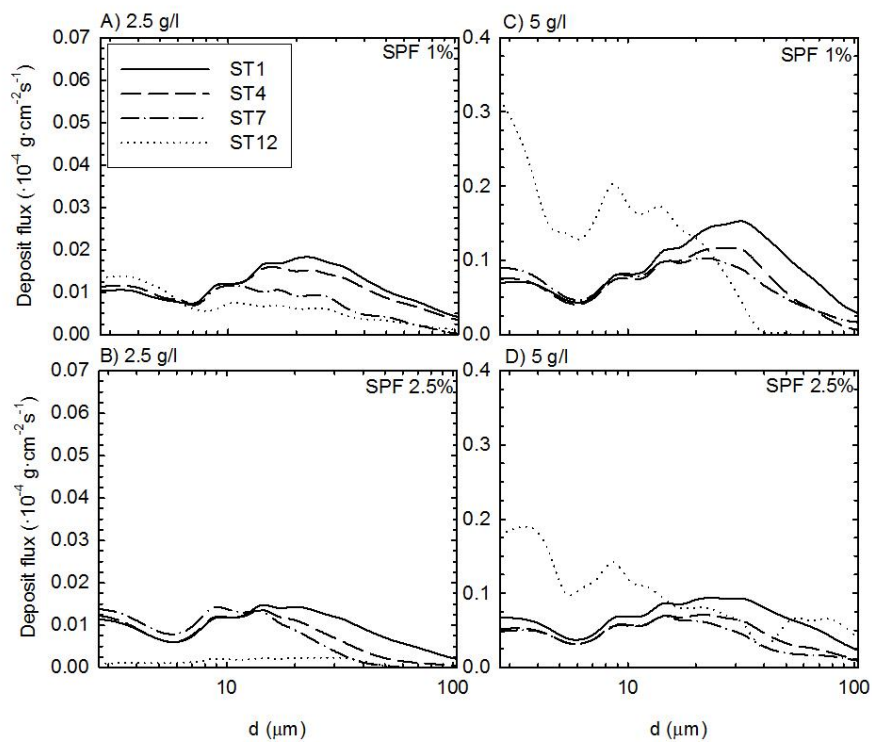


Fig. 8

1

2

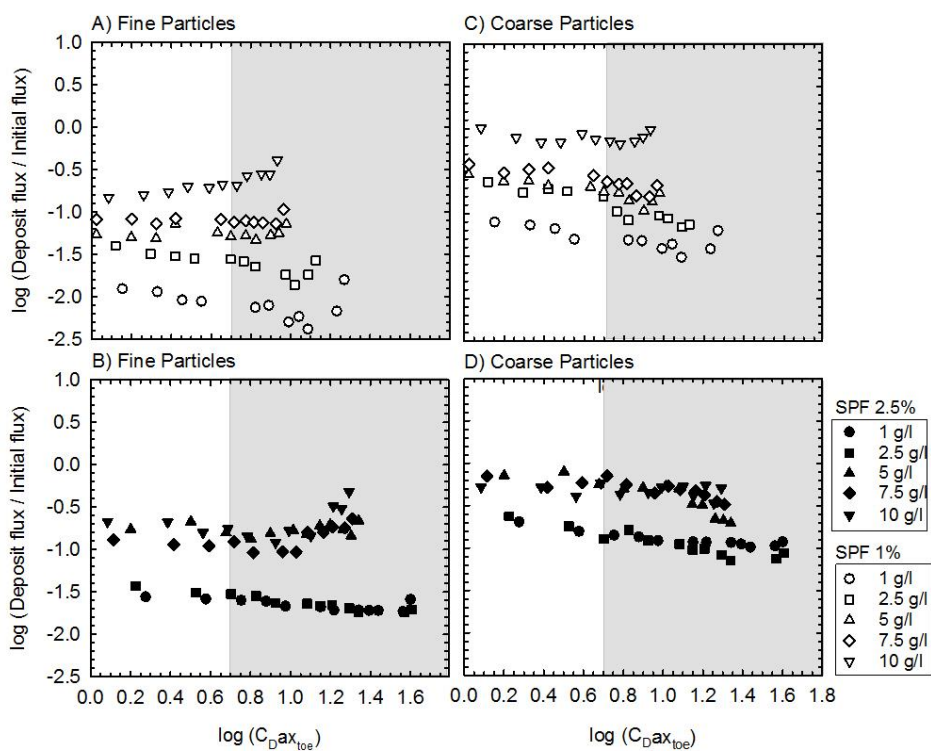


Fig. 9